EXPRESSION PROFILE OF THE BATESIAN MIMICRY GENE *DOUBLESEX* IN THE BUTTERFLY SPECIES *PAPILIO LOWI*

PHOEBE CECILE HALL

THE KRONFORST LAB
DR. MARCUS KRONFORST, DR. MEREDITH DOELLMAN

A THESIS SUBMITTED TOWARD THE DEGREE OF BACHELOR OF SCIENCE IN BIOLOGICAL SCIENCES IN THE COLLEGE OF THE UNIVERSITY OF CHICAGO

MAY 20TH, 2022

Abstract

Sexually dimorphic female-limited Batesian mimicry is known to be present in butterflies of the genus *Papilio.* The sex differentiation transcription factor *doublsex (dsx)* has been shown to act as the mimetic switch in *Papilio polytes,* and aspects of its expression and function have been studied. However, little is known about *doublsex's* function in the mimicry phenotype of a related species, *Papilio lowi.* In this study, I investigate *doublesex's* role in *Papilio lowi* through RNAi experiments on wing pattern development, antibody staining experiments on developing wings to determine expression localization, and RNAseq analysis of expression across early pupal wing development. I find that an RNAi knockout of *doublesex* in female wings yields male-type scales in the regions where *dsx* expression is knocked down. The RNAseq data shows that *doublsex* expression in development is quite different in *Papilio lowi* than it is in *Papilio polytes.* Based on antibody staining, it is evident that *doublesex* is expressed in nuclei and that this expression occurs in the regions where specific wing patterning manifests. The results of this investigation are significant for understanding how the same gene can lead to similar phenotypes in related species via molecular mechanisms which only share some similarities.

Introduction

Mimicry is a classic example of an adaptive trait across many organisms. There are three main kinds of mimicry; Self-mimicry, Müllerian mimicry, and Batesian mimicry. Self-mimicry is not characterized by a relationship between two species, instead it is when one body part resembles another. Eye spots are an example of self-mimicry. Müllerian mimicry and Batesian mimicry both involve multiple species; Müllerian mimicry involves multiple toxic species with similar warning coloration/ patterning, such that all benefit from a predator's encounter with any

one species (Müller 1876). Batesian mimicry is mimicry of a toxic species by nontoxic ones, and is considered to be a parasitic relationship (Bates 1861). The parasitic mimetic species is afforded the benefits of appearing to be dangerous without actually being toxic at all. Batesian mimicry is subject to frequency-dependent selection, as the more non-toxic mimics there are, the more predators learn that individuals with that appearance are not always dangerous (Bates 1861). The concept of Batesian mimicry was developed through the study of mimicry in Amazonian butterflies and is observed in many butterfly genera, including the swallowtail genus *Papilio* (Bates 1861).

When considering wing color patterning in butterflies, it is important to understand butterfly life cycle and developmental timing. Caterpillars hatch from fertilized eggs and grow. There are five developmental stages caterpillars go through: first instar, second instar, third instar (Figure 1A), fourth instar (Figure 1B), and fifth instar (Figure 1C). The transition between instar stages is marked by molting. From fifth instars, caterpillars pupate and become pupae or chrysalises (Figure 1E). At the start of pupation, they are considered pre-pupae (Figure 1D). The day the pre-pupae turn into pupae is day 0 of pupation, the next day would be considered day 1 of pupation, and so on. How long a butterfly is in its chrysalis before it emerges as an adult depends on the species.

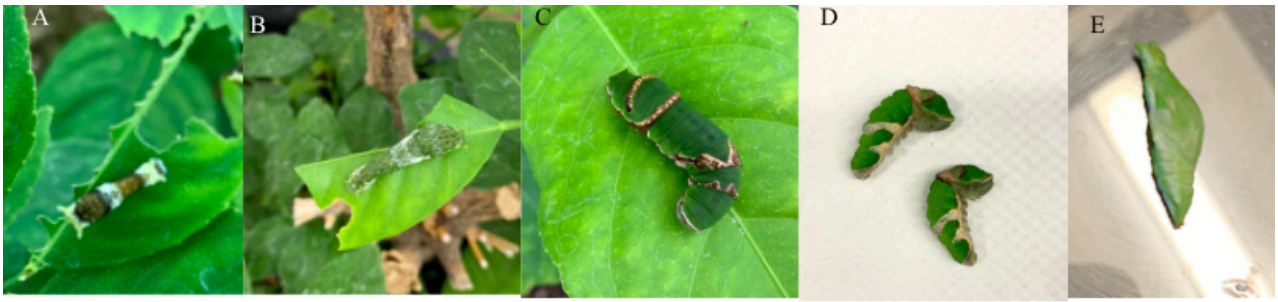

Figure 1. Developmental Stages of *papilio lowi.*
A. Third instar caterpillar. B. Fourth instar caterpillar. C. Fifth instar caterpillar. D. Pre-pupae E. Pupa

Wing imaginal discs develop from epidermal cells in caterpillars. When pupation occurs, the imaginal discs expand into a monolayer of cells making up pupal wings (Nijhout 1991). This early monolayer is not fully organized (Nijhout 1991). Patterned cell division occurs producing scale cells (butterfly wings are made up of scales), socket cells, and cells that are pre programmed for death (Nijhout 1991). These divisions are governed by Notch signaling, and lead to organized rows of scale and socket cells (Iwata et al. 2014). F-actin has been shown to help elongate the scale cells into scales in early stages of wing development and then to help organize chitin secretion to generate ridges in the scales during later wing development (Dinwiddie et al. 2014). Organization of wings into rows of scales is usually present by day 2 of pupation in *Papilio lowi* (Doellman et al in prep).

In addition to the organization of the cells there is also color patterning that occurs in pupal wing development. *WntA* and *Optix* are key genes in butterfly wing patterning. *WntA* is a signaling ligand in the *Wnt* family. It has been shown to act early in wing development to define color pattern boundaries, instead of actively depositing pigment or acting as a melanic activator (Mazo-Vargas et al 2017). *WntA* is known to have this role across many genera of butterflies, and the patterns it outlines vary by species. For example, it has a role in making stripe-like patterns in *Vanessa* butterflies (Mazo-Vargas et al 2017). Melanin pathway genes like *black, tan, ebony,* etc are known to deposit pigment in wings and the body in late stages of pupal development, and black melanin is the last to be deposited (Kuwalekar et al 2020). There is evidence that the peak in melanin pathway gene expression comes earlier in females than it does in males (Kuwalekar et al 2020). *Optix* expression is suspected to complement and fill in WntA's boundary making, as it has complementary expression to WntA but at later stages, as seen in studies with *Heliconius* butterflies (Martin et al 2012). *Optix* is a transcription factor and has been shown through

CRISPR/Cas9 experiments to be the activator of wing color which is required for pigmented coloration in butterfly wings (Zhang et al 2017). It is also responsible for structural color (iridescent blue) in some species, such as *Junonia coenia* (Zhang et al 2017). Most of these coloring genes act as trans-regulatory elements, such that genes they act on are on separate chromosomes from where they are encoded (Zhang et al 2017).

Within the genus of swallowtail butterflies *Papilio,* sexually dimorphic Batesian mimicry limited to females is present in many species. Sexual dimorphism is the existence of physical differences between males and females within the same species. The degree of sexual dimorphism depends on the species. In mimetic species of *Papilio,* males never exhibit a mimetic wing pattern, which is a form of sexual dimorphism. Batesian mimicry is subject to frequency-dependent selection, or selection where the fitness of a phenotype is governed by the frequency of that phenotype within the population. Too high a proportion of non-toxic mimics would teach predators to no longer avoid the mimetic patterning. The mimetic wing patterning which some of the Asian *Papilio* females have resembles the toxic *Pachliopta* genus of butterflies (Kunte et al 2014). Specifically, the mimetic wing pattern is mostly exhibited in the hind wing of mimetic females (Figure 2A). Some females exhibit the mimetic coloring (Figure 2A) and some exhibit patterning similar to that of the males or patterning that differs from both the males and the mimetic females (Figure 2B). The white male-type scales on the hindwings are a scale-type mostly unique to males, and these scales possess UV reflectance. Females rarely have these white, UV-reflectant scales (Figure 2 D,E).

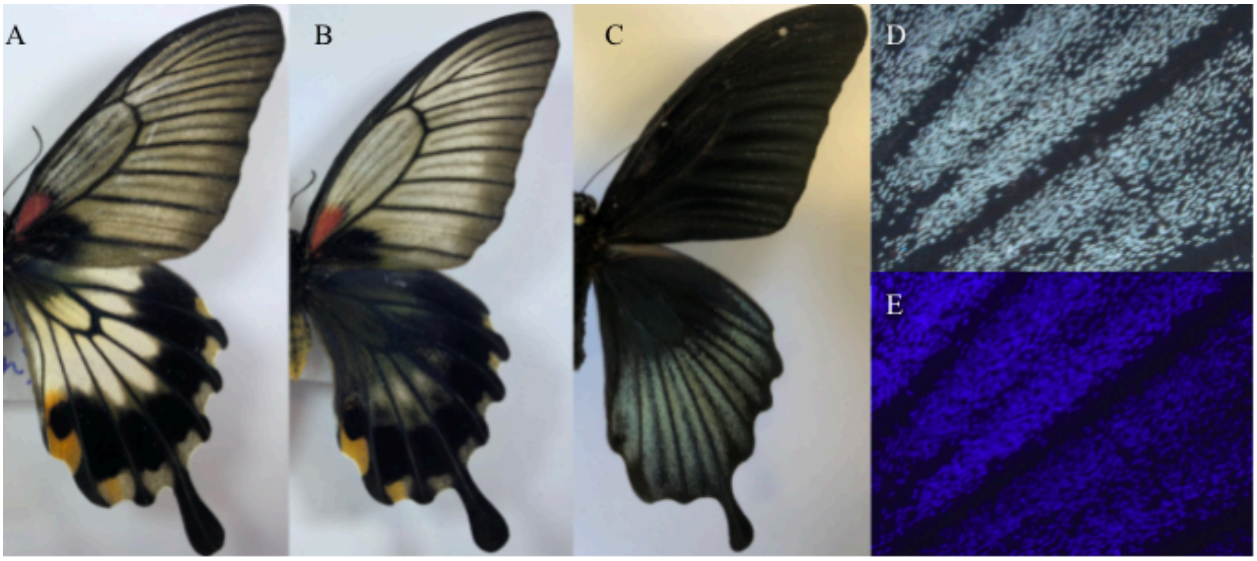

Figure 2. Wing patterns in *papilio lowi.*
A. Mimetic female. B. Non-mimetic female. C. Male D. Close-up of male-type scales on a male
E. UV reflectance in close-up of male-type scales on a male

The genetic basis of this mimicry has been the focus of much scientific inquiry (Clarke & Sheppard 1972, Black & Shuker 2019, Kunte et al 2014, Nishikawa et al 2015, Palmer & Kronforst 2020). Initial crossing experiments demonstrated that the variation in wing patterning in *Papilio polytes* is controlled by a single Mendelian autosomal locus (Clarke, Sheppard 1972). It was determined that multiple alleles at this single locus existed in a dominance hierarchy (Clarke, Sheppard 1972). Evidence that a single locus controlled the whole wing pattern led researchers to characterize the mimicry in *Papilio* as likely being supergene mimicry (Clarke, Sheppard 1960). A supergene is defined as a "cluster of physically linked genes inherited as a single unit" (Black and Shuker 2019). Supergenes may evolve when the inheritance of two or more genes together provides a fitness advantage, such that recombination is not favorable (Black and Shuker 2019). It is thought that the single locus of the supergene may be formed by a chromosomal inversion that prevents recombination thus connecting multiple adjacent genes into a single locus (Joron et al 2011). This lack of recombination is thought to be positively

associated with maintaining polymorphisms in a population since each allele of the supergene is separately maintained instead of being able to recombine with other alleles. Therefore, traits with complex balanced polymorphisms are classic candidates for supergene inheritance patterns (Black and Shuker 2019).

It was later found that the gene *doublesex (dsx)* acts as a supergene to control this mimicry phenotype in *Papilio polytes* (Kunte et al 2014). *Doublesex* had previously been known to be involved in sex determination and differentiation in insects (Shukla et al 2010, Kijimoto et al 2012), such that it is plausible that this sexually-dimorphic mimicry patterning may have evolved to co-opt this existing pathway (Kunte et al 2014). *Doublesex* pre-mRNA can be spliced differently to encode female or male transcription factors, leading to sexual differentiation. Between different insect species, *doublsex* is generally conserved as being downstream in the sex differentiation cascade such that its differential splicing depends on upstream regulators (Shukla et al 2010). These upstream regulators vary between insect species while *doublesex* is conserved downstream, leading to the consideration that the evolution of this cascade took place in "reverse order" (Shukla et al 2010). Previous studies show that *doublesex* has been co-opted for sexually dimorphic phenotypes in other insects. For example, sexual differences in beetle horns are impacted by *dsx,* as an RNAi knockdown of *dsx* reduced horn development in large males and induced horn development in generally hornless females (Kijimoto et al 2012).

Doublesex was identified as being responsible as the mimicry switch in *Papilio polytes* through multi-phase genetic mapping. Initially, bulk segregation analysis, screening, and fine-mapping indicated a 300 kb genomic region containing 5 genes, one of which was *dsx* (Kunte et al 2014). *Dsx* was then determined to be the main candidate gene since its roles in sexual differentiation were known. Comprehensive association mapping comparing mimetic and

non-mimetic individuals showed strong associations in the *dsx* region, as did a separate Genome-Wide Association Study (GWAS) (Kunte et al 2014).

In *P. polytes* mimicry wing pattern control, *doublesex* acts through classic Mendelian inheritance with the mimetic haplotype *dsx(*H*)* being dominant to the non-mimetic one (*dsx*(h)) (Nishikawa et al 2015). A female would exhibit the mimetic phenotype if she had one or more mimetic alleles of *doublesex*, but a male would never have the mimetic wing pattern, regardless of his alleles, due to the sexual dimorphism of the mimicry. Using whole genome sequencing, an autosomal inversion was identified as distinguishing mimetic and non-mimetic chromosomes from each other (Nishikawa et al 2015). Linkage mapping demonstrated this inversion as being associated with the specific mimicry locus of *dsx* within the chromosomes (Nishikawa et al 2015). The divergence between the mimetic and non-mimetic chromosomes is estimated to have occurred 40 million years ago, and since recombination is suppressed due to supergene status, the mimetic and non-mimetic alleles have diverged significantly as indels, other mutations, etc accumulate over time (Nishikawa et al 2015).

It has also been shown that RNAi knockdowns of *dsx* through injection into a developing wing of mimetic *P. polytes* female individuals yields the non mimetic wing pattern in mimetic individuals in the region where the injection occurred. This indicates that the dominant *dsx* allele governs the emergence of mimetic coloration where it is expressed in mimetic females (Nishikawa et al 2015). qPCR results showed that the mimetic form of *dsx* is highly expressed in mimetic *polytes* females during early stages of pupal development, which are key for wing development. Additionally, RNA-seq results demonstrate that the dominant *dsx* allele, *dsx*(H), is highly expressed in heterozygous *polytes* females and barely expressed in heterozygous *polytes*

males on day 2 of pupation (Nishikawa et al 2015). Taken together, these functional results link *dsx* directly to the mimetic wing pattern observed in mimetic female *Papilio polytes.*

The phenomenon of female-limited polymorphic mimicry is present across *Papilio* species, especially within the phylogeny of Southeast Asian Swallowtail *Papilio.* Subsequent analysis suggests that although female-limited mimetic wing patterns differ between species in the *Papilio* genus, all Southeast Asian *Papilio* species investigated thus far have their mimicry phenotype controlled by *dsx* (Palmer & Kronforst 2020, Iijima et al 2018). Iijima et al. conclude that in *Papilio polytes* and *Papilio memnon,* this is due to parallel evolution, and that in both species *dsx* is associated with very similar chromosomal regions. Through qPCR they found that in *P. memnon* females the mimetic allele is more strongly expressed than the non-mimetic allele, similar to in *p. polytes.* However, they found that in *P. memnon, dsx* was not contained by chromosomal inversion, which is part of what led them to believe that parallel evolution rather than an ancestral polymorphism was at play.

Palmer and Kronforst (2020) offered an updated hypothesis. Their explanation resulted from comparing genetic variation and its compatibility with hypotheses of ancestral polymorphism, hybridization, and parallel evolution (Palmer & Kronforst 2020). Independent parallel evolution would mean that the co-option of *dsx* for mimicry occurred independently in various *Papilio* species. Hybridization would result in shared mimicry alleles between species that had hybridized within the genus. Palmer and Kronforst considered ancestral polymorphism through two avenues; a simple version where different ancestral polymorphisms are passed to different species, or alternatively ancestral polymorphism with proximal allelic turnover resulting in differing mimicry gene systems in different species. Genetic analyses such as GWAS and linkage disequilibrium heat maps provided evidence for *dsx* as a mimicry supergene that

resulted from co-option of the existing *dsx* pathway leading to ancestral polymorphism which then experienced allelic turnover in different species.

This proposed evolution pattern suggests that between *Papilio* species there will be similarities in the way *dsx* governs mimicry, but also differences which will make examining the way it exhibits genetic control over the adaptive mimicry phenotype in related species fruitful. Therefore, for my thesis research I investigated the role of *dsx* in female-limited polymorphic mimicry in *Papilio lowi* in hopes to contribute to a deeper understanding of this evolutionarily significant adaptive phenomenon.

Papilio lowi is quite closely related to *Papilio memnon,* so much so that in initial work on the species, Clarke and Shepard considered *P. lowi* to be morphs of *P. memnon* that just had a different geographical distribution (Clarke and Shepard 1972). However, they have since come to be considered their own species. *Papilio lowi* have different wing patterns than *P. memnon* do. GWAS data show that wing color patterning is strongly associated with the *doublesex* locus in *lowi,* just as it is in *P. polytes* (Doellman et al. in prep). And, genetic analyses suggest that *lowi* has different mimetic and non-mimetic *doublesex* alleles than *P. memnon* does (Doellman et al. in prep).

In *Papilio lowi,* males, mimetic females, and non-mimetic females all have different wing patterns (Figure 2), whereas in *P. polytes* males and non-mimetic females look the same. This makes studying expression of *dsx* in *P. lowi* an interesting comparison to previously published data on *P. polytes.* While there is no peak expression of *dsx* in non-mimetic females nor in males of *P. polytes* (VanKuren et al. in prep), perhaps there would be in non-mimetic *lowi* females, given their different patterning from males. Thus, I investigated the role of *doublesex* in

the mimicry phenotype in *Papilio lowi.* I compared the timing of peak expression of *doublsex* in the hindwings between mimetic females, non-mimetic females, and males across early pupal development, and compared this expression profile with that of *Papilio polytes*. I focused on hindwings specifically as this is the region where the mimetic pattern comes through on the wings, and thus is likely to be where differential expression governs differential patterning. To confirm that *doublesex* is needed for the mimetic patterning in *lowi,* I performed RNA interference on the developing hindwings to knock out *doublesex* expression in that region. I also studied the localization of *doublesex* expression by using antibody staining and fluorescence microscopy. These experiments should provide useful insights into the functioning of *doublesex* in which this gene has not yet been investigated.

Methods

The overall flow of my experiments was to dissect out hindwings from *Papilio lowi* pupae of various genotypes at various stages of development (Figure 3). These hindwings were then either stained and fixed for confocal microscopy (Figure 3C) or had their RNA extracted for RNAseq analysis, making for two main experimental groups. Additionally, some individuals were not dissected as pupae but instead injected with RNAi at the start of pupation and allowed to emerge as butterflies.

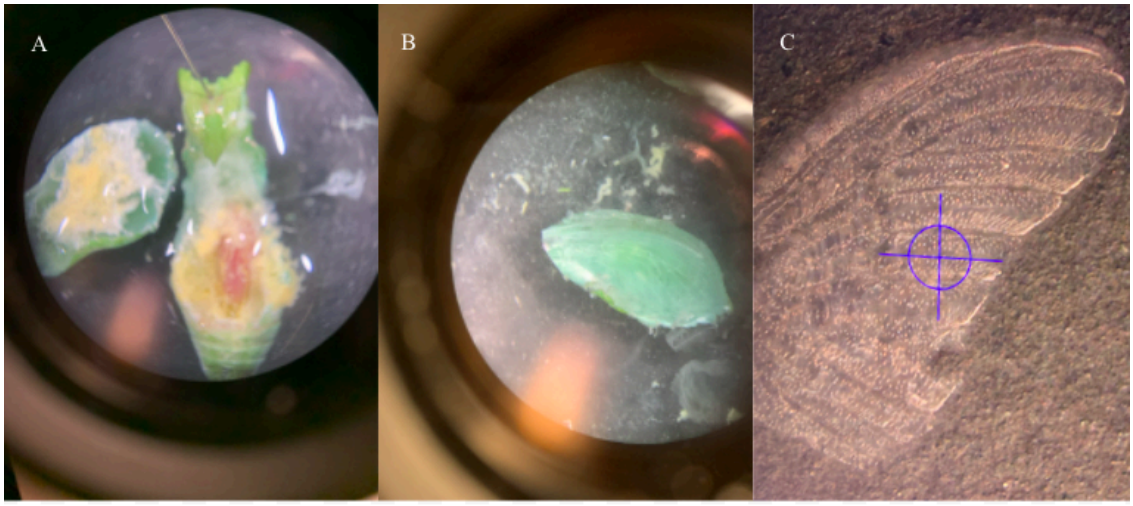

Figure 3. Dissections.
A.Pupa with cuticle and wings removed B. Dissected out cuticle with hind wing C. Dissected out pupal forewing

Genotyping

I genotyped all dissected individuals regardless of their experimental group (RNAseq versus antibody staining). Knowing the genotypes is critical for data to mean anything since I was looking for variation in expression based on genotype. Genotyping was done by taking tissue from inside the head of the developing pupae and using a quick-extraction protocol to extract the DNA followed by performing a custom TaqMan assay with allele-specific probes to determine their *dsx* genotypes. I used custom fluorescent probes for the mimetic *doublesex* allele and for the non mimetic allele, and these probes are amplified depending on the genotype of the sample. When determining genotypes of butterflies that were full grown and alive, for example ones that were to be used in crosses as parents, DNA was extracted from a single hind leg and used in the custom TaqMan assay, instead of using head tissue.

RNAi Methods

In order to observe if RNAi against *doublesex* had the same impact on mimetic wing patterning in *Papilio lowi* as it does in *Papilio polytes,* I performed *in vivo* RNAi electroporation experiments in *lowi.* These were performed on mimetic and non-mimetic female pupae on day 0 of their pupation. Following the procedure outlined in Fujiwara & Nishikawa (2016), the forewing was pulled back so that the hindwing could be accessed and a 2.0 uL injection of 10 uM or 100 uM *doublesex* DsiRNA was made into the center of the left developing hindwing. The DsiRNA targets base pairs 219-224 in exon 1 of *dsx* (5'-AGGGTCACAAGCGCTACTGCAAGTAC-3'). There are no differences between the mimetic and non-mimetic alleles in exon 1, so this injection targets all *dsx* expression (Doellman et al. in prep). A 10V electric current was run through the wing to allow the injected RNA to enter cells. The wings were then returned to their original positions and the pupa was left to continue developing normally until it emerged as an adult butterfly. The RNAi injection was made with a microinjector and a microcapillary needle.

Antibody Staining Methods

To determine where physically in the wing *dsx* is expressed, I performed antibody staining for *dsx* on wings dissected out of the developing pupae, mounted them on slides and imaged them using the confocal microscope. We used day 5 wings here because preliminary data shows that in *P. polytes* on day 5 the *dsx* expression occurs in the regions where the mimetic patterning will occur, and *P. polytes* and *P.lowi* are known to have similar development times (Van Kuren et al unpublished work). The wings were prepared for staining by being fixed using

4% formaldehyde, then blocking them using PBST with 1% BSA. The staining was done using a rabbit-anti-*dsx* custom primary polyclonal antibody raised against exons 1 and 2 of *dsx* in *P.polytes* at 1:1000 (VanKuren et al. in prep) and a goat anti-rabbit secondary antibody at 1:1000. Since exons 1 and 2 are present and translated in all isoforms of *dsx,* this stain should tag any expressed *dsx.* I also stained for DNA using DAPI and actin using Phalloidin-Alexa Fluor 555. A negative control wing was done with no primary antibody against *doublesex.* The stained wings were stored in Vectashield, then mounted on slides and imaged on the UChicago upright Zeiss Laser Scanning Microscopes (LSM) 710. To confirm that our antibody stain was specifically staining *dsx* we treated one wing from some individuals with anti-*dsx* RNAi to see if there were patches where the stain did not show up corresponding to where the RNAi injection was performed (data not shown).

RNAseq Methods

To provide individuals for experimentation, we reared three heterozygote by heterozygote crosses (crosses where the males and females each have one mimetic and one non mimetic allele of *dsx)* of *Papilio lowi*, or three biological replicates. Following these three initial crosses, we set up additional mimetic by mimetic and non-mimetic by non-mimetic crosses to fill in missing individuals given our goals for representation of all desired genotypes, sexes, and ages. The crosses were set up by placing males and females of the desired parental genotypes in butterfly cages made of netting in a greenhouse, with nectar as food for the adults and Meyer lemon plants for eggs to be laid on such that the resulting caterpillars could feed on them. The goal was to have representation in the resulting offspring of three replicates for each sex (male or female) by

age (day 0- day 4) by genotype combination (homozygous nonmimetic, homozygous mimetic, and heterozygote). Days 0 through 4 were selected because *P. lowi* has a similar pupation timeline to *P. polytes,* and *P. polytes* shows a peak in expression of *dsx* in mimetic females on day 2 of pupation. Ideally, the three biological replicates were to be from different crosses such that they had the same sex, *doublesex* genotype, and age but different parents.

To analyze the timing of the expression of *dsx* during development, I dissected out the developing wings of pupae, performed RNA extraction, and quantified and diluted these samples for RNAseq. The dissection was performed by pinning pupae in gel petri dishes, pouring Phosphate-buffered saline over them, and cutting them open around their wing cuticles (Figure 3A), then pulling the hind wing off of the forewing and cuticle with fine forceps (Figure 3B). The hind wings were then stored in 500 mL of RNAlater at -80℃ until the RNA extraction was performed. The RNA was then extracted using a Trizol reagent RNA extraction protocol. RNA pellets were then washed with 70% ethanol and resuspended in 50 mL RNAse-free water. The quantification was done with a Nanodrop and Qubit, and the dilution to normalize all samples to 100 ng/ uL for RNAseq library preparation was done using RNAse free water. This dissection and RNA extraction was done on males and females of all genotypes (homozygous mimetic, homozygous non-mimetic, and heterozygotes) across days 0 through 4 of the pupal development process. How old the pupae were when they were dissected was randomized to get an even distribution of individuals across days 0 through 4. Sometimes crosses would not have the right genotype, or RNA yield would be poor, etc. such that the number of individuals represented in

the RNAseq dataset was 58 (Table 1).

RNAseq Samples

Time point	F (M/M)	F (M/n)	F (n/n)	M (M/M)	M (M/n)	M (n/n)
Day 0	0	2	0	2	2	0
Day 1	0	2	2	0	3	0
Day 2	3	3	3	3	3	2
Day 3	1	2	3	3	3	3
Day 4	2	2	3	1	2	3

Table 1. Number of representatives of each age/ sex/ genotype class used in the RNAseq dataset.

The RNAseq library preparation and sequencing were performed at the UChicago Genomics Facility. After receiving my samples, the facility did Oligo-dT mRNA directional library prep. Then, 100 base pair paired end sequencing was performed on an Illumina NovaSeq S1 flow cell. This was done using about 30 million clusters per sample and about 60 million paired end reads per sample.

To analyze the RNAseq data, I first used the Salmon 1.2.1 package on the UChicago Gardner computing cluster to quantify gene reads in each sample (Patro 2017). This was done using a transcriptome from a non-mimetic female *P.lowi* to compare samples to. The transcriptome was assembled using TrinityRNASeq 2.10.0 (Grabherr 2011) and then annotated using Trinotate (Byrant 2017). Running the data through Salmon resulted in a quant file for each individual. These files were then read into R Studio using tx import, and subsequently converted

into a DEseq dataset. I used DESeq2 to normalize the read counts and filter the number of genes being considered to genes with at least 15 counts in at least 20 samples (Love 2014). I transformed the remaining genes using VST (variance stabilizing transformation) to compress variance in gene expression towards a common value in order to have better visualization. The resulting dataset was used for principal component analysis (PCA) and expression profiles of specific genes. For differential expression analysis, the normalized read counts were used and the design of analysis was sex + genotyoe + genotype:sex. The reference factor for genotype was set as non-mimetic and the reference factor for sex was set as male. These factors are considered the baseline in their respective categories.

Results

RNAi Results

The RNAi experiments where injected individuals were left to emerge as butterflies confirmed that a knockout of *doublesex* in developing wings of *P. lowi* females yields the male pattern in the injected region (Figure 4). In the injected region indicated by the red box in figure 4E for the mimetic female, we see that the classic black, white and orange mimetic pattern (seen on the opposite, non-injected wing) is gone and replaced by black scales interspersed with the white male-type scales. These white male-type scales can be seen up close in the injected region of the mimetic female in figures 4F and 4G. This is similar to RNAi results in *P. polytes.* However, unlike *P. polytes,* non-mimetic *P.lowi* females have their own unique pattern that is not identical to the male pattern. RNAi injected non-mimetic females show the male scale type and patterning in their injected region too, as we see black and white male-type scales in the injected region replacing the black, gray, and orange non-mimetic pattern seen on the opposite,

non-injected wing (Figure 4A). These white male-type scales in the injected region can be seen up close on the non-mimetic female in figures 4B and 4C, and in figure 4D we see that they have the same UV reflectance characteristic of these scales on the males. This presence of male-type scales in a region of *dsx* knockout on a non-mimetic female indicates that *doublesex* is not only responsible for the female mimetic wing pattern, as it is in *P. polytes,* but that it is also involved in the female-specific, non-mimetic wing patterning in *P.lowi.* In both the mimetic and non-mimetic females that had RNAi injections, specifically male-like scales (white and UV-reflectant) and patterning can be seen in the injected region (Figure 4B,C,D,F,G).

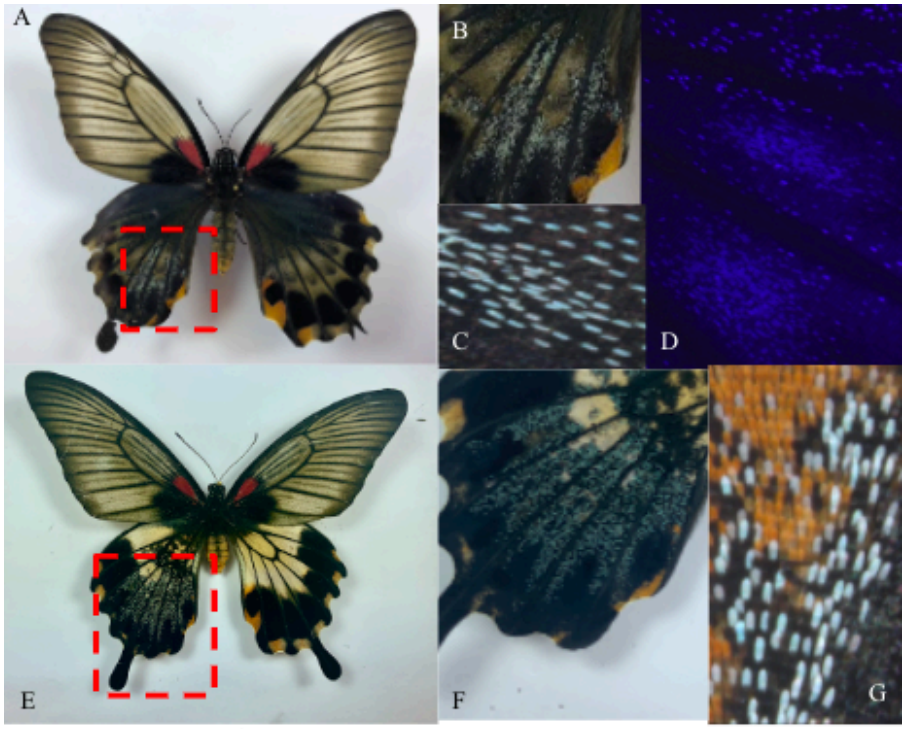

Figure 4 . RNAi Results.
A.Non-mimetic female with *doublesex* RNAi injection in left hind wing (region indicated by red outline). B. Close-up of injected region of non-mimetic female. C. Close up of male-like opal scales in RNAi injected region of non-mimetic female D. Opal male-like scales in in RNAi injected region of non-mimetic female showing UV reflectance E. Mimetic female with *doublesex* RNAi injection in left hind wing (region indicated by red outline) F,G. Close up of injected region of mimetic female, showing opal male-like scales

Antibody Staining Results

The antibody staining in a day 5 mimetic female showed that *dsx* is expressed in the nucleus of the scale and socket cells (Figure 5, 5F). This can be seen as it fully overlapped with the DNA stain in regularly arranged rows of cells. The region of the wing where this nuclear expression occurred appears to be the region of the hindwing that is patterned white in a mimetic female (Figure 5B,C,D). The same trends can be seen in a heterozygous female (Figure 6). Additionally, it can be seen in both the mimetic and heterozygous females that the orange regions in the mimetic patterning have *dsx*, while the black circle between the white and orange regions (outlined by the red box, Figure 5C, E, Figure 6C,E) does not show *dsx* staining. In a non-mimetic female (Figure 7), it is evident that *dsx* is expressed in the regions of the wing that will develop a scale color other than black, as can be seen by comparing Figure 7B with Figure 7D. This is also the case in terms of the scale color fates of regions where *dsx* is expressed in mimetic females, but the *dsx* stain outline varies depending on the mimetic and non-mimetic patterns.

The staining results in both a heterozygous (Figure 8) and a mimetic male (Figure 9) show that there is no *dsx* expression in the wing, and certainly not any in an organized pattern as we see in the homozygous mimetic and the heterozygous females. The faint staining that is visible is noise, not *dsx.* This is confirmed because when the stained sections of the male wing are zoomed in on, the color does not show up in nuclei as with the female stains, but instead shows up as flecks of color around the cells. Additional confirmation that the male staining is noise, not *dsx,* comes from the fact that we performed RNAi against *dsx* on a mimetic male wing prior to staining it (Figure 9 D,E,F). The injection was performed on the lower right quadrant of the wing as displayed in Figure 9, and can be seen as a hole in the wing where the needle

punctured it. If the *dsx* stain were real, the staining should disappear around the injection site where the RNAi knocked down expression, but this is not the case.

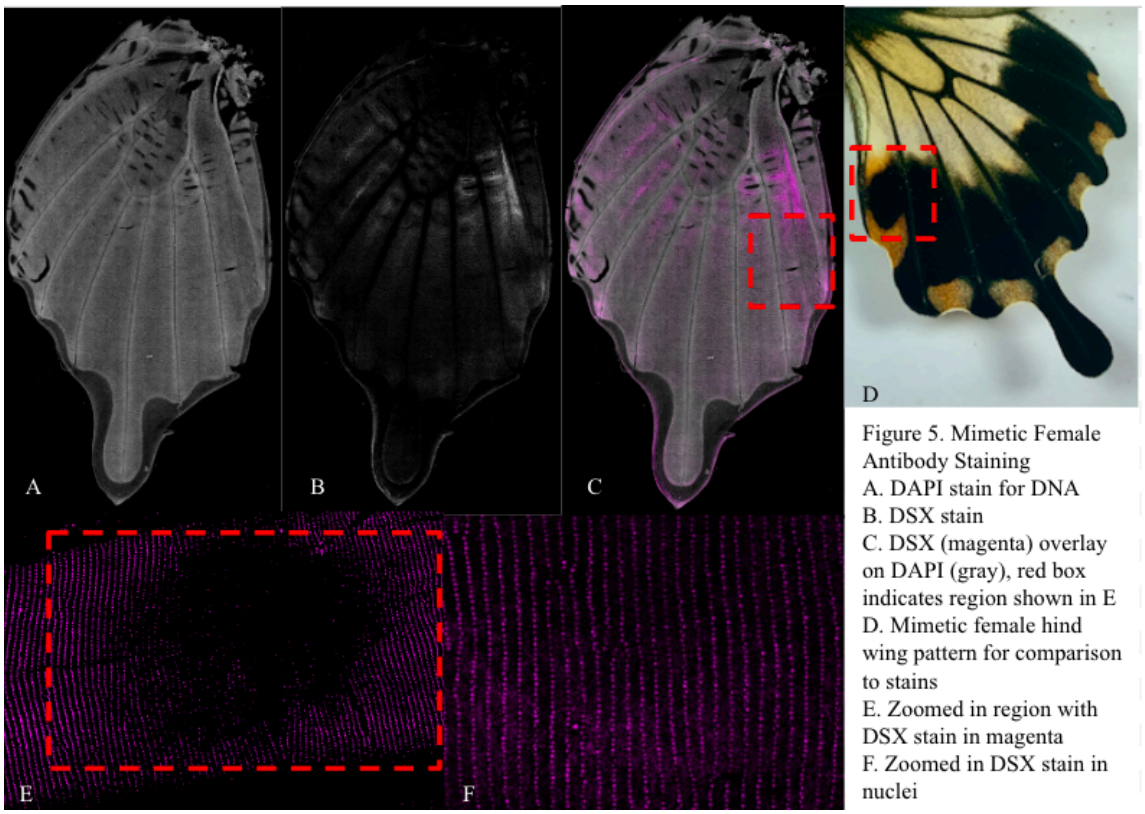

Figure 5. Mimetic Female Antibody Staining
A. DAPI stain for DNA
B. DSX stain
C. DSX (magenta) overlay on DAPI (gray), red box indicates region shown in E
D. Mimetic female hind wing pattern for comparison to stains
E. Zoomed in region with DSX stain in magenta
F. Zoomed in DSX stain in nuclei

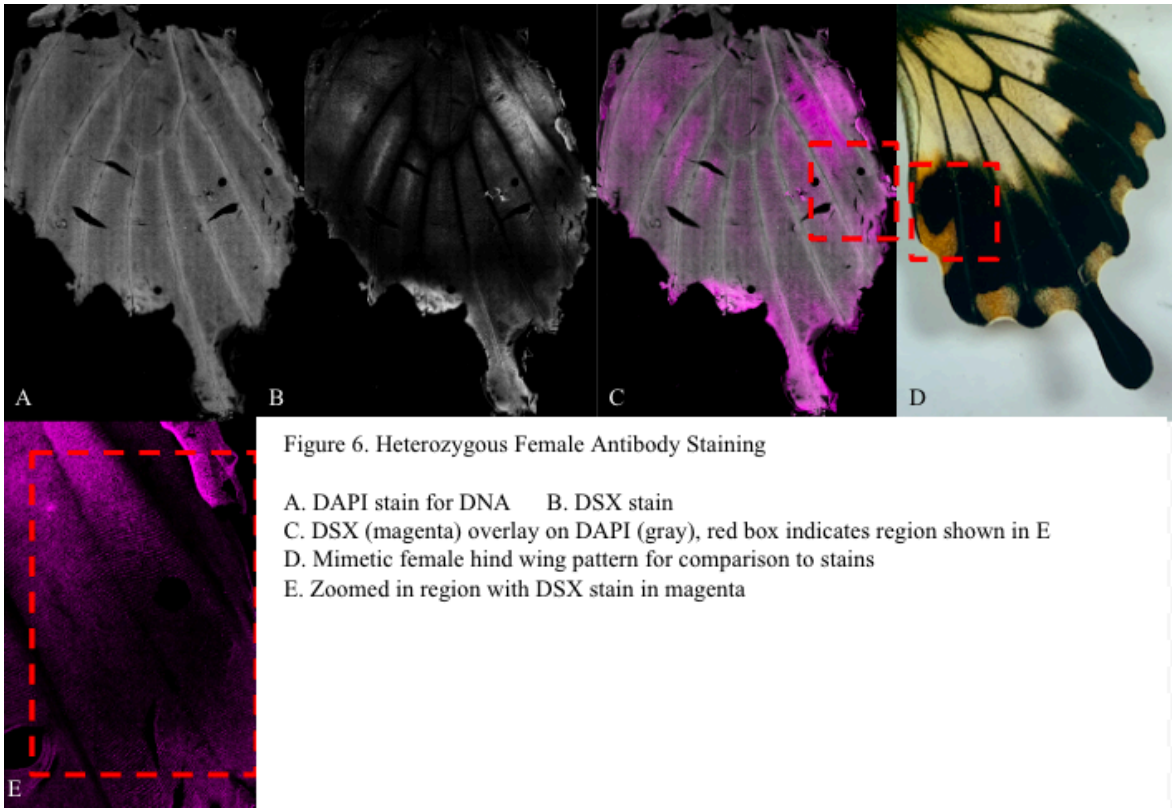

Figure 6. Heterozygous Female Antibody Staining

A. DAPI stain for DNA B. DSX stain
C. DSX (magenta) overlay on DAPI (gray), red box indicates region shown in E
D. Mimetic female hind wing pattern for comparison to stains
E. Zoomed in region with DSX stain in magenta

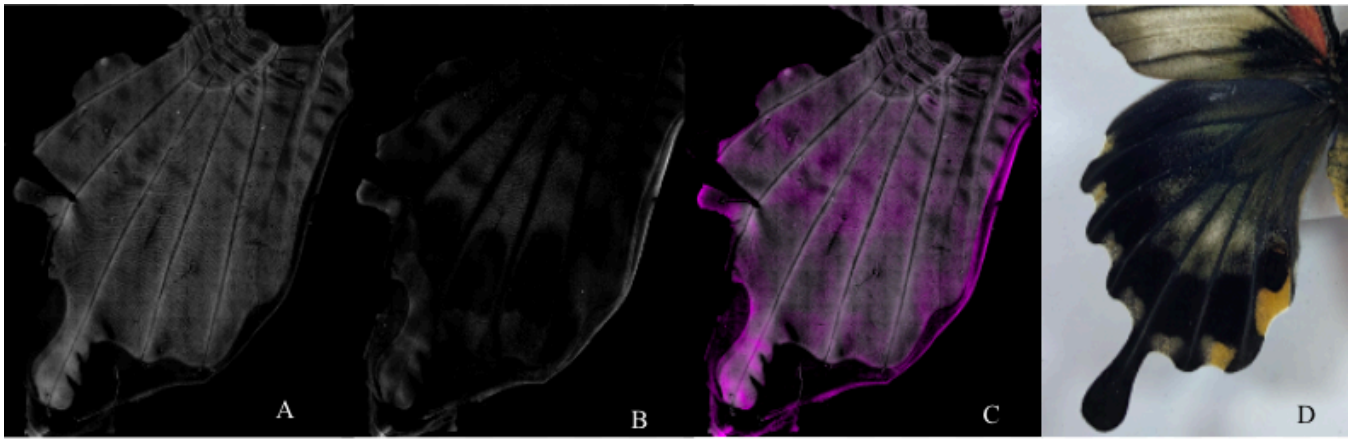

Figure 7. Non-mimetic Female Antibody Staining
A. DAPI stain for DNA B. DSX stain C. DSX (magenta) overlay on DAPI (gray)
D. Non-mimetic female hindwing pattern for comparison to stains

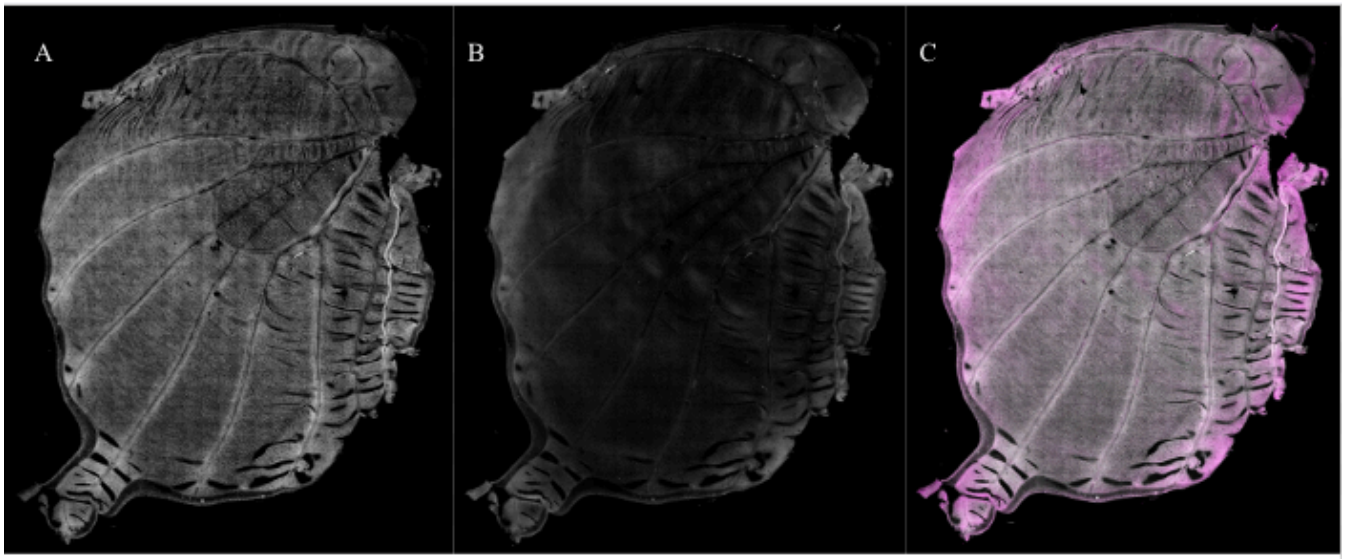

Figure 8. Heterozygous Male Antibody Staining
A. DAPI stain for DNA
B. DSX stain
C. DSX (magenta) overlay on DAPI (gray)

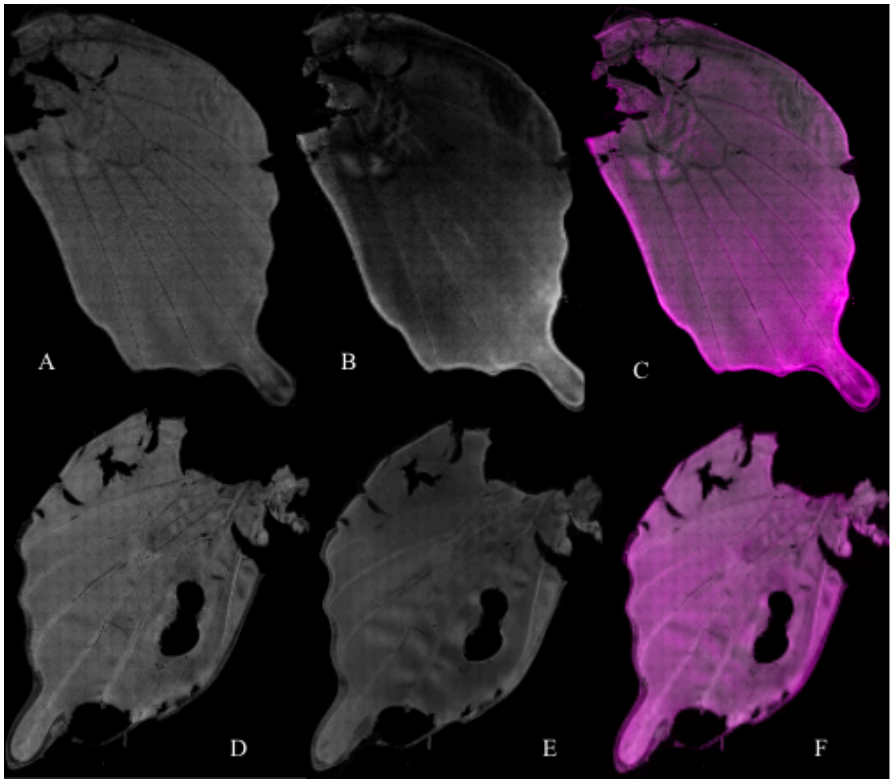

Figure 9. Mimetic Male Left and Right Wings, *dsx* RNAi in left wing

A,B,C: non-injected wing:
A. DAPI stain for DNA
B. DSX stain
C. DSX (magenta) overlay on DAPI (gray)

D,E,F: injected wing
D. DAPI stain for DNA
E. DSX stain
F. DSX (magenta) overlay on DAPI (gray)

RNAseq Results

Several results came out of the RNAseq data set. When considering gene expression overall, instead of expression of any specific genes, samples were ordered by day along PC1, which accounted for 22% of the variation in gene expression across the whole data set (Figure 10). This evident grouping was not the case for grouping by sex by age or sex by genotype or genotype, etc. Thus, in the PCA individuals are clustered by shape as denoting developmental stage, but the colors representing sex by genotype (non- mimetic males (nM), non-mimetic females (nF), heterozygous males (hM), heterozygous females (hF), mimetic males (MM), and mimetic females (MF) show no clustering.

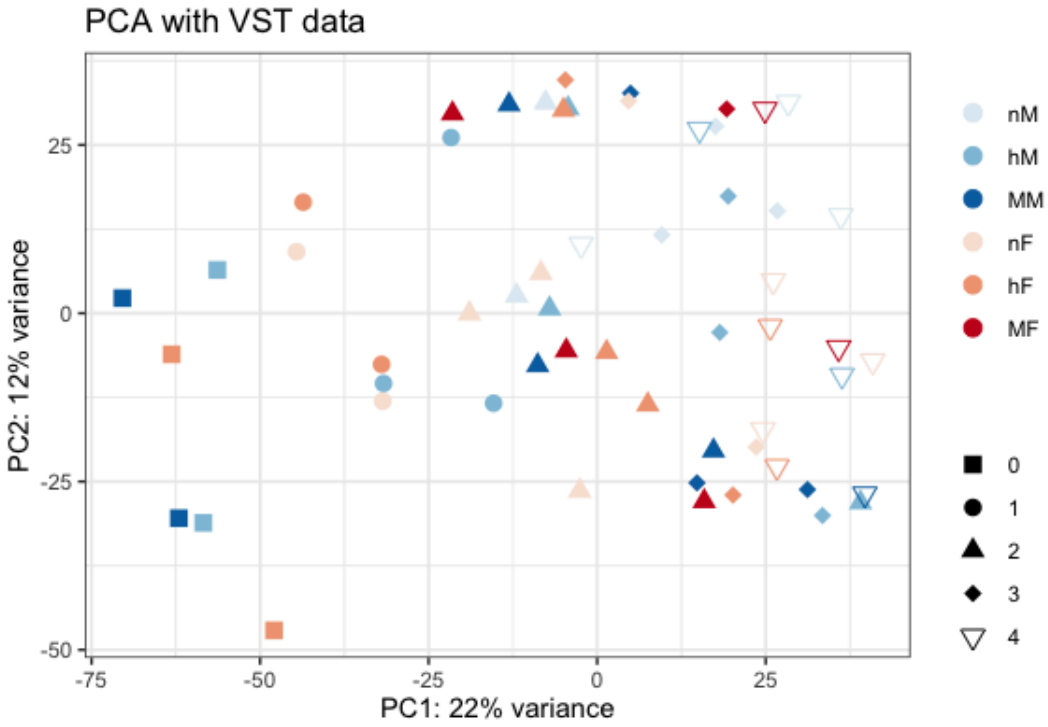

Figure 10. PCA by Stage (indicated by shape), with sex and genotype indicated by color.

When analyzing specifically *doublsex* expression, a peak in mimetic females was expected on day 2, as that is the case for *P. polytes* (VanKuren et al. in prep). My data show that the expression profile of *doublesex* is quite different in *P. lowi* than it has been shown to be in *P. polytes* (Figure 11). The expression data were analyzed using genotype by sex groupings plotted across days (Figure 11). The expression profile shows *dsx* transcript abundance (counts) versus age of pupae for the sex by genotype classes. No specific class of individuals shows any trend that is distinct in comparison to other groups, unlike in *P. polytes* where mimetic females had a unique peak at over 2000 *dsx* transcripts (VanKuren et al. in prep). In my results, all counts of *dsx* transcripts are between 100 and 300, with no significant increase in expression during a particular time, or no expression peaks. For *P. polytes,* all other genotypes, sexes, and days besides day 2 mimetic females had counts around 100. Thus, in my results, basically all counts are slightly elevated, but none have extreme peaks.

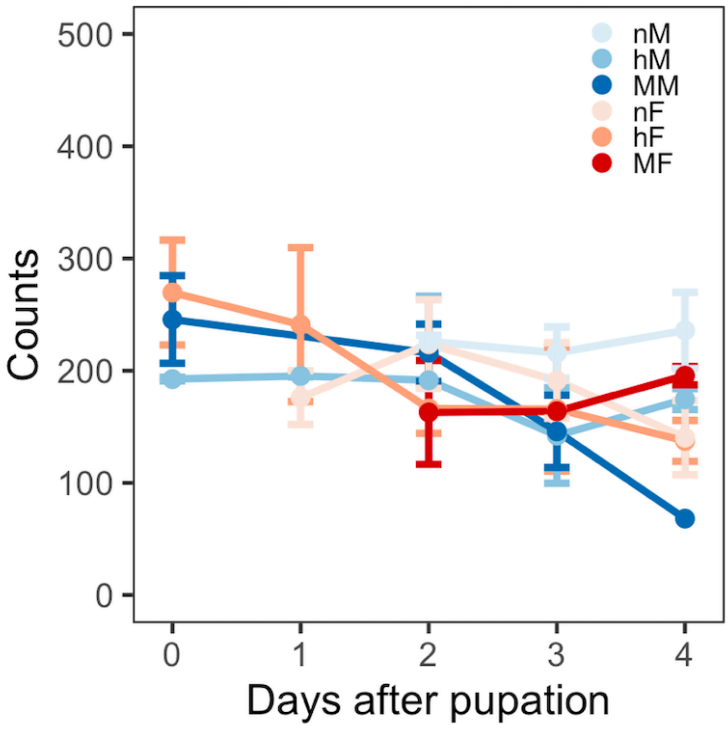

Figure 11. *dsx* expression over development.

Differential expression analyses showed the effects on females of being either heterozygous or homozygous mimetic on gene expression as compared to the baseline of being non-mimetic (Figure 12). Thus, we see that on day 2 there are many differentially expressed upregulated genes for both mimetic and heterozygous females. Additionally, we see that homozygous mimetic females have many differentially expressed genes on day 4. When considering just the effect of being female, regardless of genotype (Figure 12C), we see that there are many differentially expressed genes between the sexes on day 4. For days 2 and 4, significantly differentially expressed genes between heterozygous or mimetic females and non-mimetic females are shown graphically in volcano plots, with a p-value plotted on the y-axis with a significance cut-off of $p < 0.1$, and fold change in expression on the x-axis (Figures 13-16). Red data points indicate significantly differentially expressed genes in that they meet our p-value cut off of $p \leq 0.1$ and meet the default log fold change in expression, whereas black data points do not meet both these standards. The higher a datapoint is on the y-axis the more significant its p-value. The transcript IDs of these data points can be matched to the tables of significantly expressed genes sorted by p-value (Tables S1-S3). Since in Figure 10 we see that at day 3, females have no significant differentially expressed genes, thus there are no day 3 volcano plots.

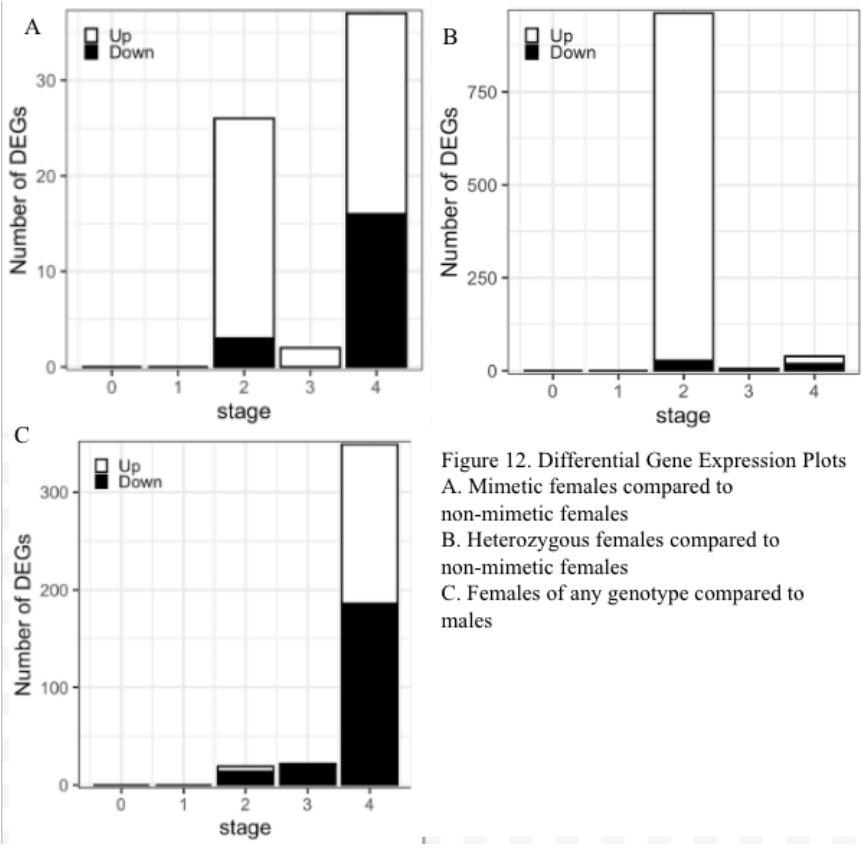

Figure 12. Differential Gene Expression Plots
A. Mimetic females compared to non-mimetic females
B. Heterozygous females compared to non-mimetic females
C. Females of any genotype compared to males

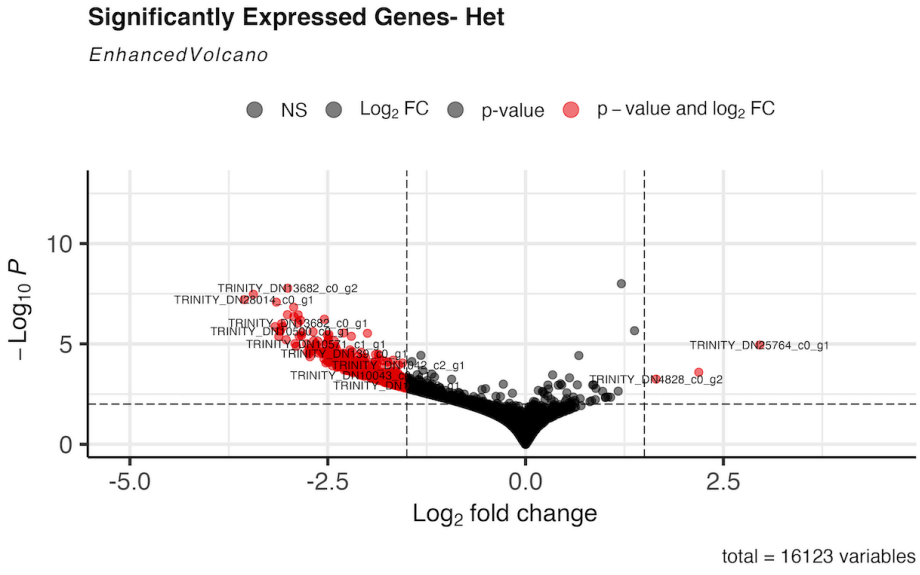

Figure 13. Volcano plot for significantly differentially expressed genes in day 2 heterozygous females.

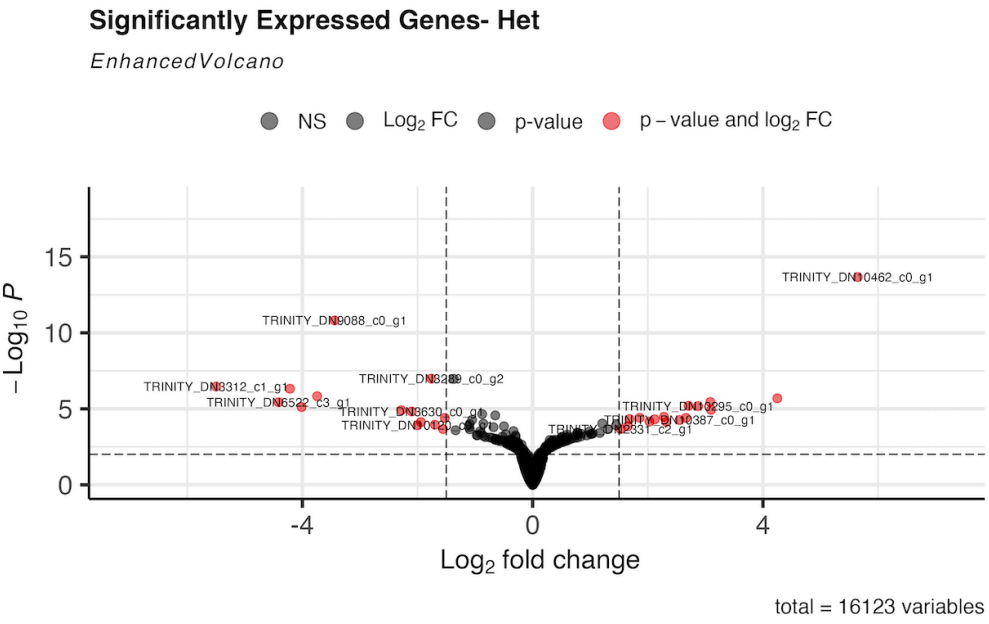

Figure 14. Volcano plot for significantly differentially expressed genes in day 4 heterozygous females.

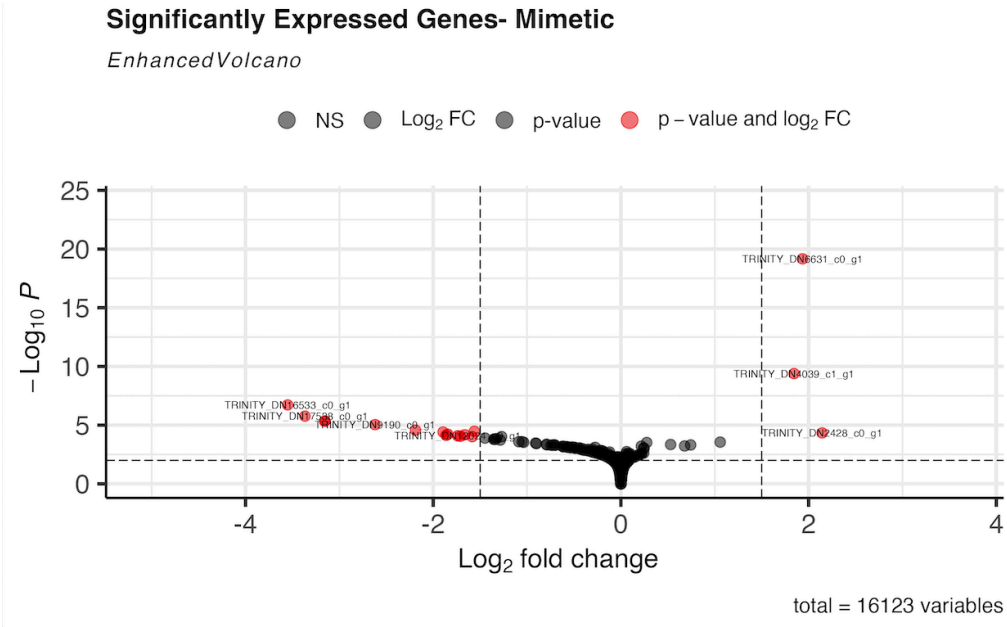

Figure 15. Volcano plot for significantly differentially expressed genes in day 2 mimetic females.

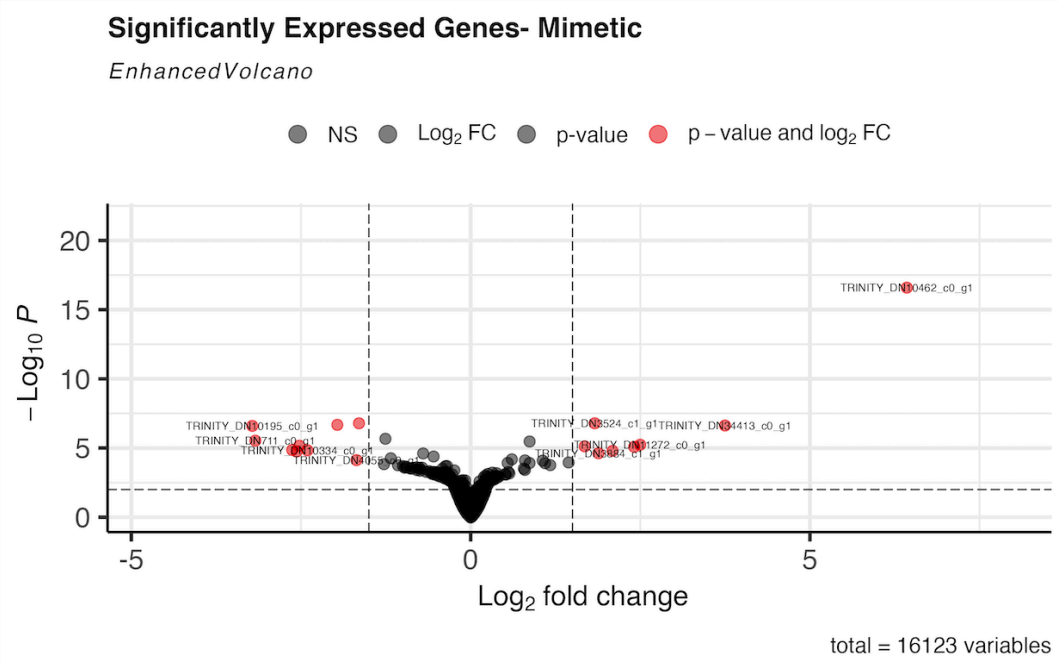

Figure 16. Volcano plot for significantly differentially expressed genes in day 4 mimetic females.

There is overlap between specifically which genes are differentially expressed ($p \leq 0.1$) in homozygous mimetic females and heterozygous females on each day of development (Figure 17). On day 2, 26 genes were significantly differentially expressed in mimetic females, and all of those 26 genes were also significantly differentially expressed in heterozygous females, which also had 941 non-overlapping significantly differentially expressed genes (Figure 17A, Table S1, S2). Day 4 mimetic and heterozygous females had 7 overlapping significantly expressed genes, with mimetic females also having 30 non-overlapping significantly expressed genes, and heterozygous females also having 33 non-overlapping significantly expressed genes (Figure 17C, Table S3).

Some of the genes that were significantly differentially expressed in day 2 females of both the mimetic and heterozygous genotypes are implicated in wing development processes. The gene *tld* is significantly upregulated on day 2 in both mimetic and heterozygous females.

This gene is known in *Drosophila* to be involved in wing vein development as derived from imaginal discs, in addition to being implicated in dorsal-ventral patterning (The UniProt Consortium 2022, Anston 2022). In heterozygous day 2 females, *unk* or RING finger protein unkempt is significantly upregulated, and this gene is known to be required for normal wing development, as a knockout results in "unkempt" flies with incorrectly oriented wings (Mohler et al 1992). Additionally, *wapl* or protein wings apart-like, is significantly downregulated, and is known to suppress *white* and enhance *brown* position-effect variegation and is involved in female meiotic chromosome segregation (Verní et al 2000). The genes *brown* and *white* are involved in the transport of dark pigment precursor molecules into pigment cell granules (The UniProt Consortium 2022, Verní et al 2000). Helicase domino or *dom,* which is required for wing disc pattern formation, is also upregulated in day 2 heterozygous females (Gause et al 2006). By day 4 of development, genes involved in coloration and melanization are significantly expressed in females. The gene *yellow-f2,* related to *yellow,* is significantly expressed in day 4 females, and is known to be involved in the melanization and melanin synthesis pathways (Han et al 2002, The UniProt Consortium 2022). Knockdowns of this gene result in decreased melanin synthesis (Han et al 2002, The UniProt Consortium 2022).

Interestingly, none of the significantly differentially expressed genes found in *P. polytes* wing development RNAseq experiments are found to be differentially expressed in this *Papilio lowi* dataset. In *Papilio polytes,* it was found that genes such as *engrailed, invected, wnt 1, wnt 4, wnt 6, wnt A*, and *groucho* were significantly upregulated in developing hindwings, and were specifically upregulated at the same time points as with *doublesex* (VanKuren et al unpublished work). However, *wingless* is in the *wnt* pathway, and the gene *sfl* or Bifunctional heparan sulfate

N-deacetylase/N-sulfotransferase is significantly upregulated in heterozygous day 2 *lowi* females and is known to be required for the diffusion of *wingless.*

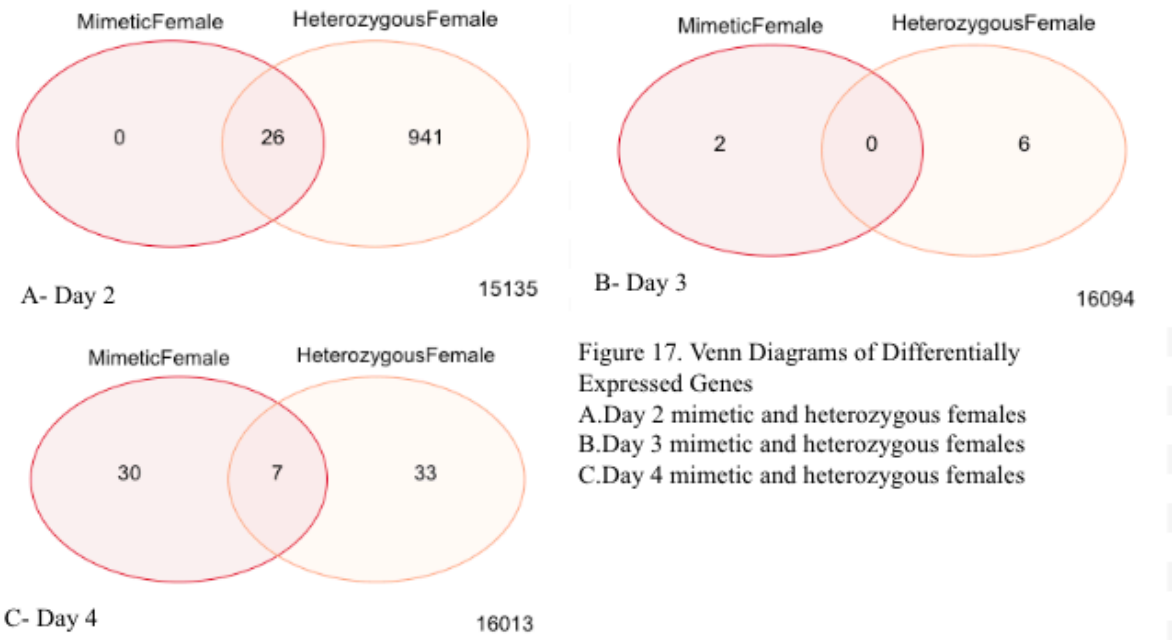

Figure 17. Venn Diagrams of Differentially Expressed Genes
A.Day 2 mimetic and heterozygous females
B.Day 3 mimetic and heterozygous females
C.Day 4 mimetic and heterozygous females

Discussion

Many of these results are significant for our understanding of *doublesex's* mechanisms of governing mimicry in *P. lowi.* The RNAi results indicating that a knockdown of *dsx,* or functionally an absence of *doublesex,* results in the male-type pattern and scales in both phenotypes of female (mimetic and non-mimetic females) means that likely the male-type pattern and scales are a base-line or default for wing patterning which the expression of *doublesex* overrides. The fact that *dsx* is needed for the non-mimetic female phenotype as well complicates our understanding of *dsx* as the "mimicry switch." This broader implication for its roles in the co-opted mimicry switch, on top of its ancestral role in sexual dimorphism (Shukla et

al 2010), would not have been discoverable in a species like *P. polytes* which has no unique non-mimetic female phenotype. This validates this work being done in *P. lowi.*

The antibody staining results complement and shed further light on this situation. Seeing that in the mimetic and non-mimetic females *dsx* expression occurs in the shape of the lightly colored regions of mimetic and non-mimetic patternings, respectively, indicates that the way that *doublesex* overrides the male-type default patterning is directly through expression in the regions which are destined to not exhibit male-type scales in the mimetic patterning. Since mimetic and non-mimetic females end up with different coloration in the regions where we see the *dsx* stains, it is likely that *dsx* activates different genes or functions differently molecularly in some way such that the expression pattern does not manifest in the same color pattern. *Doublesex* is known to be a transcription factor (Shukla et al 2010), and indeed in the staining we see that it is present in the nucleus as would be expected of a transcription factor. The fact that we see no specific nor patterned *dsx* staining in the male wings provides further evidence that the expression of *dsx* in hindwings leads to mimetic patterning since in the males which never exhibit the mimetic patterning there is no patterned *dsx* expression.

The RNAseq results provide a lot of insight. The PCA clustering by day of development matches expectations since it is a comparison of expression of all genes, not specifically *dsx.* So, for example, logically a day 2 individual would be expressing similar genes to other day 2 individuals, and be expressing less similar genes as compared to a day 4 individual. Thus, the PCA serves as a bit of a sanity check, as the data points really should be clustering by day considering what is known about developmental gene expression in general.

The RNAseq results illuminate an expression profile for *dsx* in *P. lowi* that is unique compared to that of *P. polytes* in a number of ways. These results showing a lack of expression

peak potentially are logical considering that *P. lowi* has non-mimetic females that are distinct from males, and that their patterning is also governed by *dsx* (as shown in my RNAi experiments). Therefore, perhaps *dsx* has a higher baseline across all classes because of its involvement in all classes including the unique non-mimetic female patterning. This potentially means that *dsx* is governing patterning in different ways in *P. lowi* than it does in *P. polytes.* The lack of a peak in expression in any class of individuals from days 0-4 and the fact that none of the co-expressed genes in *P. lowi* match any of these genes in *P. polytes* demonstrate that the molecular mechanism differs, and suggests that the peak in *dsx* expression in mimetic females may come later in development in *P. lowi* than it does in *P. polytes*. Since *dsx* is known to be a transcription factor, and we do not see any of the co-upregulated genes from *polytes* being significantly upregulated in *P. lowi,* perhaps in *P. lowi dsx* acts as a transcription factor on a different set of genes.

The genes that are significantly upregulated in both mimetic and heterozygous females can provide insights into which genes are required to make the mimetic phenotype since both of these genotypes have the mimetic phenotype. There is the greatest number of genes overlapping in significant expression between these genotypes on day 2 of development as seen in the venn diagrams, which likely means day 2 of pupation is significant for mimetic patterning, even if there isn't a huge peak in *dsx* expression itself on that day. Having the greatest number of overlapping significantly differentially expressed genes in day 2 is a similarity to *P. polytes* (VanKuren et al. in prep).

The significant down-regulation of genes involved in making dark pigments— *yellow-f2* and *wapl* (Han et al 2002, Verní et al 2000)—in females, which will exhibit the mimetic phenotype, is a very important result. The mimetic phenotype has far more white patches than

the non-mimetic female phenotype and the male phenotype. Thus, the downregulation of genes which deposit dark pigment makes a lot of sense. Since the antibody staining shows that *dsx* is expressed in the white and light patches, it could be that *dsx* is responsible for down regulating these dark pigment genes in the regions which will become white.

Conclusions

This research has illuminated key aspects of the role and functioning of the gene *dsx* in *P. lowi.* It is clear that *dsx* is required for both the mimetic female hindwing patterning and the non-mimetic female hindwing patterning, since the RNAi knockdown of it produced male-type scales in both genotypes of female. It seems that *dsx* governs this patterning through expression specifically in the regions of the hindwing where the mimetic and non-mimetic females develop non-black scales, as demonstrated by the antibody staining results. Where the functioning of *dsx* seems to differ in *P. lowi* as compared to *P. polytes* is in its expression profile across wing development. Instead of having a peak at day 2 in mimetic females, as is the case in *P. polytes,* here I find that the expression is consistent across all classes of individuals without any one having an extreme peak of expression. This may be expected considering the significant role that *dsx* also plays in non-mimetic females, as shown by the RNAi and antibody staining results.

There is room for further investigation into what other genes may be coexpressed, and/or have their expression impacted by *dsx.* It would be especially interesting to investigate this further with the genes *yellow-f2* and *wapl* which are down-regulated dark pigment genes. Additionally, getting more individuals as representatives of each timepoint for each genotype and sex combination would be beneficial for an even larger dataset. And, considering the lack of a distinct peak in expression in mimetic females it could be worth extending the stages that are

included in the dataset to see if perhaps there is a peak, just later in development. Staining across days of development would also be quite interesting to see if the expression of *dsx* is always in the regions of the mimetic and non-mimetic non-black pattern or whether it is expressed in other regions in earlier or later stages of development. Overall, this work has yielded key findings surrounding *doublesex's* role in *P. lowi's* mimicry, and how the timing of expression and molecular function of this protein vary in *P. lowi* as compared to the previously investigated species *P. polytes.* This shared role of the same gene accomplished through different avenues in related species is evolutionarily significant.

References

Antson, Hanna et al. “The developing wing crossvein of Drosophila melanogaster: a fascinating model for signaling and morphogenesis.” *Fly* vol. 16,1 (2022): 118-127. doi:10.1080/19336934.2022.2040316

Bates, Henry Walter. “Contributions to an Insect Fauna of the Amazon Valley : Lepidoptera : Heliconidae / by Henry Walter Bates, Esq..” 1861, https://doi.org/10.5962/bhl.title.9486.

Black, Daniella, and David M. Shuker. “Supergenes.” *Current Biology*, vol. 29, no. 13, 2019, https://doi.org/10.1016/j.cub.2019.05.024.

Bryant, D.M., Johnson, K., DiTommaso, T., Tickle, T., Couger, M.B., Payzin-Dogru, D., Lee, T.J., Leigh, N.D., Kuo, T.H., Davis, F.G. and Bateman, J., 2017. “A tissue-mapped axolotl de novo transcriptome enables identification of limb regeneration factors”. Cell reports, 18(3), pp.762-776.

Clarke, C A, and P M Sheppard. “Super-Genes and Mimicry.” *Heredity*, vol. 14, no. 1-2, 1960, pp. 175–185., https://doi.org/10.1038/hdy.1960.15.

Clarke; Sheppard.The genetics of the mimetic butterfly Papilio polytes. *Philosophical Transactions of the Royal Society of London.* Series B, Biological Sciences. 263(855):431-458; The Royal Society, 1972.,]

Dinwiddie, April, et al. “Dynamics of F-Actin Prefigure the Structure of Butterfly Wing Scales.”

Developmental Biology, vol. 392, no. 2, 2014, pp. 404–418., https://doi.org/10.1016/j.ydbio.2014.06.005.

Fujiwara, Haruhiko, and Hideki Nishikawa. “Functional Analysis of Genes Involved in Color Pattern Formation in Lepidoptera.” *Current Opinion in Insect Science*, vol. 17, 2016, pp. 16–23., https://doi.org/10.1016/j.cois.2016.05.015.

Gause, Maria et al. “Nipped-A, the Tra1/TRRAP subunit of the Drosophila SAGA and Tip60 complexes, has multiple roles in Notch signaling during wing development.” *Molecular and cellular biology* vol. 26,6 (2006): 2347-59. doi:10.1128/MCB.26.6.2347-2359.2006

Grabherr, M., Haas, B., Yassour, M. *et al.* Full-length transcriptome assembly from RNA-Seq data without a reference genome. *Nat Biotechnol* 29, 644–652 (2011). https://doi.org/10.1038/nbt.1883

Iijima et al. Parallel evolution of Batesian mimicry supergene in two Papilio butterflies, P. polytes and P. memnon. Science Advances. 2018. 4. 10.1126/sciadv.aao5416.

Iwata, Masaki, et al. “Real-Time in Vivo Imaging of Butterfly Wing Development: Revealing the Cellular Dynamics of the Pupal Wing Tissue.” *PLoS ONE*, vol. 9, no. 2, 2014, https://doi.org/10.1371/journal.pone.0089500.

Joron, Mathieu, et al. “Chromosomal Rearrangements Maintain a Polymorphic Supergene Controlling Butterfly Mimicry.” *Nature*, vol. 477, no. 7363, 2011, pp. 203–206., https://doi.org/10.1038/nature10341.

Kijimoto, Teiya, et al. “Diversification of *Doublesex* Function Underlies Morph-, Sex-, and Species-Specific Development of Beetle Horns.” *Proceedings of the National Academy of Sciences*, vol. 109, no. 50, 2012, pp. 20526–20531., https://doi.org/10.1073/pnas.1118589109.

Kuwalekar, Muktai, et al. “Molecular Evolution and Developmental Expression of Melanin Pathway Genes in Lepidoptera.” *Frontiers in Ecology and Evolution*, vol. 8, 2020, https://doi.org/10.3389/fevo.2020.00226.

Kunte K et al. doublesex is a mimicry supergene. Nature. 2014 Mar 13;507(7491):229-32. doi: 10.1038/nature13112. Epub 2014 Mar 5. PMID: 24598547.

Love MI, Huber W, Anders S (2014). “Moderated estimation of fold change and dispersion for RNA-seq data with DESeq2.” *Genome Biology*, **15**, 550. doi: 10.1186/s13059-014-0550-8.

Martin, Arnaud, et al. “Diversification of Complex Butterfly Wing Patterns by Repeated Regulatory Evolution of a *Wnt* Ligand.” *Proceedings of the National Academy of*

Sciences, vol. 109, no. 31, 2012, pp. 12632–12637., https://doi.org/10.1073/pnas.1204800109.

Mazo-Vargas, Anyi, et al. "Macroevolutionary Shifts of *Wnta* Function Potentiate Butterfly Wing-Pattern Diversity." *Proceedings of the National Academy of Sciences*, vol. 114, no. 40, 2017, pp. 10701–10706., https://doi.org/10.1073/pnas.1708149114.

Mohler, J et al. "The embryonically active gene, unkempt, of Drosophila encodes a Cys3His finger protein." *Genetics* vol. 131,2 (1992): 377-88. doi:10.1093/genetics/131.2.377

Müller, Fritz. "Mimicry in Butterflies Explained by Natural Selection." *The American Naturalist*, vol. 10, no. 9, 1876, pp. 534–536., https://doi.org/10.1086/271732.

Nijhout, HF. The development and evolution of butterfly wing patterns. *Washington: Smithsonian Institution Press.* 1991.

Nishikawa H et al. A genetic mechanism for female-limited Batesian mimicry in Papilio butterfly. Nat Genet. 2015 Apr;47(4):405-9. doi: 10.1038/ng.3241. Epub 2015 Mar 9. PMID: 25751626.

Palmer DH, Kronforst MR. A shared genetic basis of mimicry across swallowtail butterflies points to ancestral co-option of doublesex. Nat Commun. 2020 Jan 3;11(1):6. doi:

10.1038/s41467-019-13859-y. PMID: 31900419; PMCID: PMC6941989.

Patro, R., Duggal, G., Love, M. I., Irizarry, R. A., & Kingsford, C. (2017). Salmon provides fast and bias-aware quantification of transcript expression. Nature Methods.

Han, Qian et al. “Identification of Drosophila melanogaster yellow-f and yellow-f2 proteins as dopachrome-conversion enzymes.” *The Biochemical journal* vol. 368,Pt 1 (2002): 333-40. doi:10.1042/BJ20020272

Shukla, J. N., and J. Nagaraju. “Doublesex: A Conserved Downstream Gene Controlled by Diverse Upstream Regulators.” *Journal of Genetics*, vol. 89, no. 3, 2010, pp. 341–356., https://doi.org/10.1007/s12041-010-0046-6.

The UniProt Consortium. “UniProt: the universal protein knowledgebase in 2022”. *UniProt.* Nucleic Acids Res. 49:D1 (2022).

Vernì, F et al. “Genetic and molecular analysis of wings apart-like (wapl), a gene controlling heterochromatin organization in Drosophila melanogaster.” *Genetics* vol. 154,4 (2000): 1693-710. doi:10.1093/genetics/154.4.1693

Zhang, Linlin, et al. “Single Master Regulatory Gene Coordinates the Evolution and Development of Butterfly Color and Iridescence.” *Proceedings of the National Academy*

of Sciences, vol. 114, no. 40, 2017, pp. 10707–10712.,

https://doi.org/10.1073/pnas.1709058114.

Table S1. Significantly Expressed Genes- Day 2 Mimetic Females

gene	log2FoldChange	padj	weight	sprot_Top_BLASTX_hit	eggnog
TRINITY_DN6631_c0_g1	1.961183592	2.23E-15	0.493345713	KLH21_BOVIN^KLH21_BOVIN^	ENOG410XNX8^kelch-like
TRINITY_DN4039_c1_g1	1.893779854	2.01E-05	0.163522877	.	.
TRINITY_DN16533_c0_g1	-4.250031705	0.000688619	1.493345713	APLP_MANSE^APLP_MANSE^	.
TRINITY_DN17538_c0_g1	-4.253772508	0.002122	3.272996143	.	.
TRINITY_DN20991_c0_g1	-4.171575867	0.002584354	4.831846777	APLP_MANSE^APLP_MANSE^	.
TRINITY_DN28014_c0_g1	-4.132764459	0.002584354	5.371137919	.	.
TRINITY_DN9190_c0_g1	-3.250022497	0.027652368	0.757104869	APLP_MANSE^APLP_MANSE^	.
TRINITY_DN13682_c0_g2	-2.561599714	0.04770215	1.493345713	TLD_DROME^TLD_DROME^	ENOG410ZPX7^MeprinA
TRINITY_DN14238_c0_g2	-4.341088232	0.04770215	5.371137919	.	.
TRINITY_DN9549_c0_g1	-2.474106224	0.06916229	1.545992286	.	.
TRINITY_DN4973_c0_g1	-3.756271684	0.072358297	3.272996143	.	.
TRINITY_DN12024_c0_g1	-2.980085817	0.073735507	1.493345713	.	.
TRINITY_DN31273_c0_g1	-4.412134987	0.08043408	1.493345713	APLP_MANSE^APLP_MANS	.

				E^	
TRINITY_DN1230_c0_g1	-2.927379871	0.08078176	0.36360663	PTP69_DROME^PTP69_DROME^	COG5599^proteintyrosinephosphatase
TRINITY_DN3661_c0_g1	-2.592281507	0.08078176	3.177913747	K1109_MOUSE^K1109_MOUSE^	ENOG410XT7P^kiaa1109
TRINITY_DN55_c0_g2	-2.709883923	0.08078176	1.493345713	SPTN2_RAT^SPTN2_RAT^	COG5069^Microtubuleassociatedmonoxygenase;calponinandLIMdomaincontaining
TRINITY_DN5549_c0_g1	-3.055579516	0.08078176	1.07864747	PO210_RAT^PO210_RAT^	ENOG410XNNU^nucleoporin
TRINITY_DN186_c0_g3	-3.375864572	0.08252424	0.757104869	.	.
TRINITY_DN8029_c0_g1	-1.948613366	0.08252424	0.36360663	SYNE1_HUMAN^SYNE1_HUMAN^	☐ COG5069^Microtubuleassociatedmonoxygenase;calponinandLIMdomaincontaining
TRINITY_DN20716_c0_g1	-3.457050531	0.092374893	1.493345713	APLP_LOCMI^APLP_LOCMI^	.
TRINITY_DN24652_c0_g1	3.195494508	0.092374893	4.831846777	.	.

TRINITY_DN6937_c0_g1	-1.966685232	0.092374893	0.76783322	DCR1_DROME^DCR1_DROME^	COG0571^DigestsdoubleстрandedRNA.InvolvedintheprocessingofprimaryrRNAtranscripttoyieldtheimmediateprecursorstothelargeandsmallrRNAs(23Sand16S).AlsoprocessessomemRNAs;andtRNAswhentheyareencodedintherRNAoperon(Bysimilarity)
TRINITY_DN21420_c0_g1	-2.514429186	0.092940535	5.371137919	LRP2_RAT^LRP2_RAT^	ENOG410XP34^beta-amyloidclearance
TRINITY_DN28689_c0_g1	-2.996990398	0.092940535	3.272996143	.	.
TRINITY_DN4864_c6_g1	-2.427720168	0.092940535	3.177913747	MYO9A_HUMAN^MYO9A_HUMAN^	COG5022^myosinheavychain
TRINITY_DN128_c4_g1	-2.407578815	0.099886753	3.272996143	C1GLT_DROME^C1GLT_DROME^	ENOG410YRJG^Core1synthase;glycoprotein-N-acetylgalactosamine3-beta-galactosyltransferase;1
TRINITY_DN128_c4_g1	-2.407578815	0.099886753	3.272996143	.	.

Table S2. Significantly Expressed Genes- Day 2 Heterozygous Females

https://docs.google.com/spreadsheets/d/1sI4Cp6Z8XFIk7hYX1TtEqzD992bXN_vA0_pI_mbTJ-E/edit?usp=sharing

Table S3. Significantly Expressed Genes- Day 4 Females

gene	log2FoldChange	padj	weight	sprot_Top_BLASTX_hit	eggnog
TRINITY_DN10462_c0_g1	6.966480501	3.37E-13	1.227994482	DCXR_CAEEL^DCXR_CAEEL^	ENOG410XQCY^)-reductase
TRINITY_DN3289_c0_g2	-1.743052962	0.00071368	1.227994482	DJC28_HUMAN^DJC28_HUMAN^	ENOG410ZU5V^DnaJ(Hsp40)homolog;subfamilyC;member28
TRINITY_DN3524_c1_g1	1.935637633	0.00071368	1.223280152	.	.
TRINITY_DN34413_c0_g1	4.558315012	0.000952401	1	.	.
TRINITY_DN28226_c0_g1	-2.0946879	0.000993721	0.685191171	PPAE_BOMMO^PPAE_BOMMO^	COG5640^protease
TRINITY_DN711_c0_g1	-4.108892539	0.003562087	2.216067179	.	.
TRINITY_DN1202_c2_g2	-1.494228765	0.006054143	0.816171374	.	.
TRINITY_DN11272_c0_g1	3.095408339	0.009454925	1.227994482	RTJK_DROFU^RTJK_DROFU^	.
TRINITY_DN5673_c0_g1	3.066543078	0.010221821	1.431384408	.	ENOG4111JFX^glutamine rich2
TRINITY_DN7	-3.19995079	0.011010909	1	.	.

191_c1_g1					
TRINITY_DN4039_c1_g1	2.046661075	0.011103327	1	.	.
TRINITY_DN10334_c0_g1	-3.377945317	0.018459885	0.914317504	.	.
TRINITY_DN10995_c0_g3	-3.952544767	0.018459885	0.927577646	.	.
TRINITY_DN9685_c0_g1	2.810029368	0.018459885	1	.	.
TRINITY_DN9685_c0_g1	2.810029368	0.018459885	1	TRET1_APILI^TRET1_APILI^	.
TRINITY_DN8364_c5_g1	-4.166710203	0.018909181	1	.	.
TRINITY_DN3884_c1_g1	7.259685123	0.019628385	1.227994482	.	ENOG4112AP6^familywithsequencesimilarity179;memberA
TRINITY_DN3884_c1_g1	7.259685123	0.019628385	1.227994482	.	.
TRINITY_DN2088_c0_g1	-1.099998535	0.038922701	1	.	.
TRINITY_DN2088_c0_g1	-1.099998535	0.038922701	1	RGP1_BOVIN^RGP1_BOVIN^	ENOG410YESN^RGP1retrogradegolgitransporthomolog(S.cerevisiae)
TRINITY_DN1040_c1_g1	-1.237838474	0.040723121	0.541671461	.	.
TRINITY_DN6914_c0_g1	-1.964579422	0.0466924	1	CP9E2_BLAGE^CP9E2_BLAGE^	.
TRINITY_DN6914_c0_g1	-1.964579422	0.0466924	1	.	.

TRINITY_DN12226_c0_g1	1.959433343	0.053529841	1.223280152	.	.
TRINITY_DN2672_c2_g2	8.187759959	0.058054067	0.914317504	.	.
TRINITY_DN28376_c0_g1	2.282091534	0.058054067	1.431384408	.	.
TRINITY_DN4055_c0_g1	-3.81958114	0.058054067	0.927577646	.	.
TRINITY_DN5073_c0_g2	1.26147573	0.058054067	0.816171374	.	.
TRINITY_DN5073_c0_g2	1.26147573	0.058054067	0.816171374	PPCS_HUMAN^PPCS_HUMAN^	COG0452^Phosphopantothenoylcysteinedecarboxylase
TRINITY_DN5073_c0_g2	1.26147573	0.058054067	0.816171374	PPCS_YEAST^PPCS_YEAST^	.
TRINITY_DN931_c0_g1	3.590633406	0.058054067	1.227994482	.	.
TRINITY_DN6160_c0_g1	1.278772865	0.060878902	1.223280152	.	.
TRINITY_DN6160_c0_g1	1.278772865	0.060878902	1.223280152	GDE_CANLF^GDE_CANLF^	COG3408^Glycogendebranchingenzyme
TRINITY_DN6160_c0_g1	1.278772865	0.060878902	1.223280152	TIGD4_HUMAN^TIGD4_HUMAN^	ENOG4110CDI^tiggertransposableelementderived
TRINITY_DN15123_c2_g1	-2.079871398	0.083882964	1.847948658	.	.
TRINITY_DN174_c0_g1	-2.606032465	0.083882964	1.223280152	GLOV_HYACE^GLOV_HYACE^	.
TRINITY_DN12515_c0_g1	-3.786600397	0.095655686	1.431384408	MTAP2_RAT^MTAP2_RAT^	ENOG4111J07^Microtubule-associatedpro

					tein
TRINITY_DN12515_c0_g1	-3.786600397	0.095655686	1.431384408	MAP4_MOUSE^MAP4_MOUSE^	ENOG4111J07^Microtubule-associatedprotein
TRINITY_DN1531_c0_g1	-3.407312245	0.095655686	0.685191171	.	.
TRINITY_DN21196_c0_g1	-4.547025897	0.095655686	0.927577646	.	.
TRINITY_DN2331_c2_g1	3.517108457	0.095655686	1.847948658	.	.
TRINITY_DN2355_c0_g2	3.894803415	0.095655686	0.846478457	.	.
TRINITY_DN25671_c0_g1	-4.510414208	0.095655686	1.431384408	.	.
TRINITY_DN31543_c0_g1	-2.729398544	0.095655686	1.223280152	LYS_BOMMO^LYS_BOMMO^	ENOG4111QHM^thoseintissuesandbodyfluidsareassociatedwiththemonocyte-macrophagesystemandenhancetheactivityofimmunoagents
TRINITY_DN5507_c0_g1	-4.569970638	0.095655686	1.227994482	CCCP_DROYA^CCCP_DROYA^	ENOG4110N42^circadianrhythm
TRINITY_DN890_c0_g1	-3.40621496	0.095655686	1.431384408	YELF2_DROME^YELF2_DROME^	ENOG410YB1P^melaninbiosyntheticprocessfromtyrosine
TRINITY_DN8	-3.40621496	0.095655686	1.431384408	.	.

90_c0_g1					